CASE 3: RANS AND URANS APPLICATION WITH CFL3D

C. L. Rumsey

Computational Modeling & Simulation Branch, NASA Langley Research Center, Hampton, VA 23681-2199

Solution Methodology

This case was run using CFL3D, a multi-zone Reynolds-averaged Navier-Stokes code developed at NASA Langley [1]. It solves the thin-layer form of the Navier-Stokes equations in each of the (selected) coordinate directions. It can use 1-to-1, patched, or overset grids, and employs local time step scaling, grid sequencing, and multigrid to accelerate convergence to steady state. In time-accurate mode, CFL3D has the option to employ dual-time stepping with subiterations and multigrid, and it achieves second order temporal accuracy.

CFL3D is a finite volume method. It uses third-order upwind-biased spatial differencing on the convective and pressure terms, and second-order differencing on the viscous terms; it is globally second-order spatially accurate. The flux difference-splitting (FDS) method of Roe is employed to obtain fluxes at the cell faces. It is advanced in time with an implicit three-factor approximate factorization method.

Model Description

For this test case, three different turbulence models were used. The first is the one-equation Spalart-Allmaras model (SA) [2], the second is the two-equation shear-stress transport model of Menter (SST) [3, 4], and the third is an explicit algebraic stress model (EASM-ko) in k-ω form [5]. The first two models are both linear eddy-viscosity models that make use of the Boussinesq eddy-viscosity hypothesis, whereas the EASM-ko is a nonlinear model. The equations describing these three models can be found in their respective references.

In CFL3D, the models are implemented uncoupled from the mean-flow equations. They are solved using a three-factor implicit approximate factorization approach. The advection terms are discretized with first-order upwind differencing. The production source term is solved explicitly, while the advection, destruction, and diffusion terms are treated implicitly. For EASM-ko, the nonlinear terms are added to the Navier-Stokes equations explicitly.

Implementation and Case Specific Details

Three flow conditions are computed over the hump model: (1) no flow control, (2) steady suction flow control, and (3) oscillatory synthetic jet flow control. The control is applied near $x/c = 0.65$ on the back side of the hump, near where the flow separates in the un-controlled state. The freestream Mach number is $M = 0.1$, and the Reynolds number is approximately Re = 936,000 per hump chordlength. For the oscillatory case, the oscillation frequency is 138.5 Hz.

All computations performed for this case were 2-D. The grid used was the supplied 2-D structured grid number 1 (which contains 4-zones connected in a 1-to-1 fashion, and approximately 210,000 grid points), as well as a medium-level grid made from the fine grid by extracting every-other point in each coordinate direction (2-D structured grid number 2). The SA model was solved on both the fine and medium grids, whereas the SST and EASM-ko models were only solved on the medium grid. For the oscillatory case, only the SA model on the fine grid was used.

For the no-flow-control and steady suction cases, CFL3D was run in steady-state mode, utilizing local time-stepping to accelerate convergence. For the oscillatory case, the time step chosen yielded 360 time

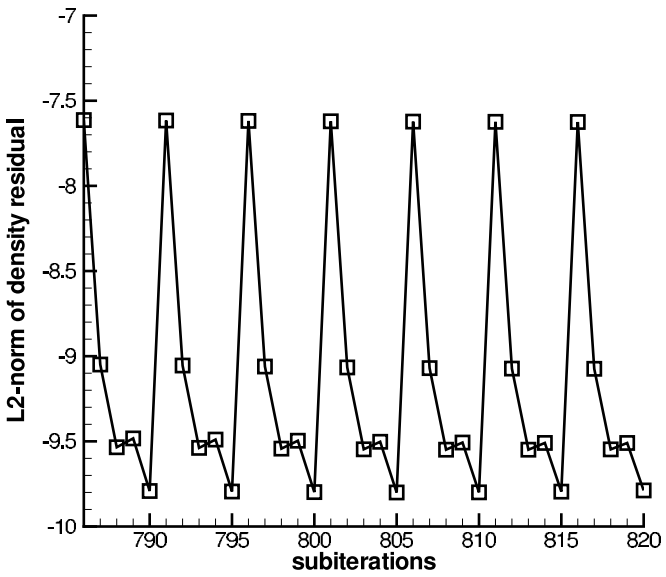

Figure 1: Convergence of subiteration residual during time-accurate oscillatory computation, SA model, fine grid.

steps per cycle of the forcing frequency, and 5 subiterations were employed per time step. For this case, this number of subiterations was enough to reduce the L_2-norm of the subiteration density residual by about 2 orders of magnitude. See Fig. 1, which shows subiteration residual over the course of 7 time steps (with 5 subiterations per time step) during part of the unsteady cycle.

The boundary conditions were as follows. At the floor and hump surfaces, as well as at the side walls inside the cavity, solid wall adiabatic boundary conditions were applied. At the front of the grid, which extended to $x/c = -6.39$, far-field Riemann-type boundary conditions were applied. At the downstream boundary (at $x/c = 4.0$) the pressure was set at $p/p_{\rm ref} = 0.99947$, and all other quantities were extrapolated from the interior of the domain. This back pressure was determined via trial and error, to achieve approximately the correct inflow conditions. At the bottom of the cavity, different boundary conditions were applied depending on the case. For the no-flow-control case, this wall was treated as an inviscid wall. For the steady suction case, the boundary condition set the velocity components as follows:

$$U = 0 \qquad V = (\rho V)_{\rm set}/\rho \tag{1}$$

and $(\rho V)_{\rm set}$ was chosen in order to achieve the equivalent of a mass flow of 0.01518 kg/s through a 23-inch span. The value used turned out to be $(\rho V)_{\rm set} = -.001248\rho_{\rm ref}a_{\rm ref}$, where $a_{\rm ref}$ is the reference speed of sound. For the oscillatory flow case, the boundary condition set the velocity components as follows:

$$U = 0 \qquad V = [(\rho V)_{\rm max}/\rho]cos(2\pi Ft) \tag{2}$$

where F is the frequency and t is the time, and $(\rho V)_{\rm max}$ was chosen in order to achieve a maximum velocity magnitude near to the target of approximately 26.6 m/s out of the slot during the cycle. Fig. 2 shows the velocity magnitude at a position near the center of the slot exit as a function of nondimensional time, on a line even with the hump surface, over the course of one cycle of oscillation. The value of $(\rho V)_{\rm max}$ used to achieve this condition was $(\rho V)_{\rm max} = 0.001\rho_{\rm ref}a_{\rm ref}$. Along with the above boundary conditions given by

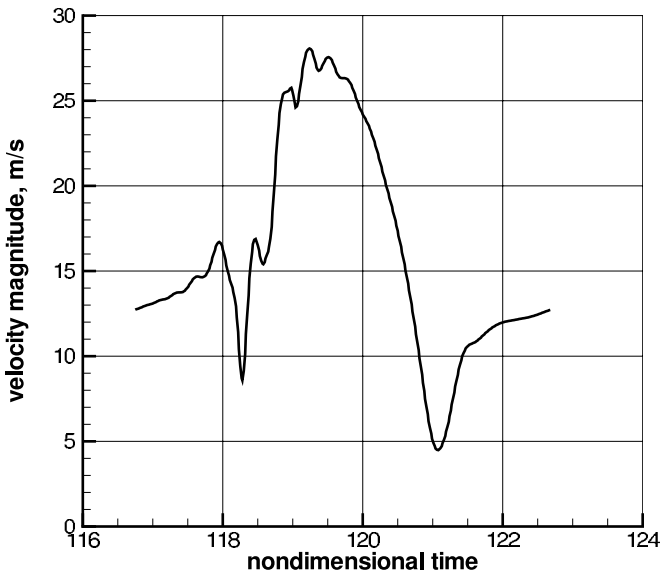

Figure 2: Velocity magnitude at the slot exit for oscillatory case, SA model, fine grid.

Eqs. 1 and 2, the density and pressure at the bottom of the cavity are extrapolated from the interior of the domain.

The top tunnel wall was treated as an inviscid wall for all of the computations submitted to the workshop. However, the effect of making the top wall a viscous wall was also investigated (using a different grid with appropriate finer normal spacing near the top wall). Resulting surface pressure coefficients are shown in Fig. 3. Using viscous top wall lowers the peak C_p levels over the center of the hump, in better agreement with experiment. However, the effect does not fully account for the difference between CFD and experiment. Also, the viscous upper wall does not impact the C_p levels in the separated region to any significant degree.

As a nonlinear model, EASM-ko can do a better job predicting the turbulent normal stresses than linear models. This can be seen in Fig. 4, which shows results predicted by the three models at $x/c = -2.14$. The linear models show no perceptible difference between $\overline{u'u'}$ and $\overline{v'v'}$, whereas EASM-ko does predict a normal stress difference. The $\overline{u'u'}$ from EASM-ko is in better agreement with the experiment, although its peak near the wall is still too low. There were no measurements of $\overline{v'v'}$.

Examples of the effects of grid and turbulence model can be seen in Fig. 5. This figure shows streamwise velocity profiles in the separated region at $x/c = 0.8$ for the suction case, using SA on both the fine and medium grids, and using SST and EASM-ko on the medium grid. There is essentially no difference between the SA results on the fine and medium grids, and the two-equation models both predict a qualitatively different profile than SA at this location.

References

[1] Krist, S. L., Biedron, R. T., and Rumsey, C. L., "CFL3D User's Manual (Version 5.0)", NASA TM-1998-208444, June 1998.

[2] Spalart, P. R., and Allmaras, S. R., "A One-Equation Turbulence Model for Aerodynamic Flows," *La Recherche Aerospatiale*, No. 1, 1994, pp. 5–21.

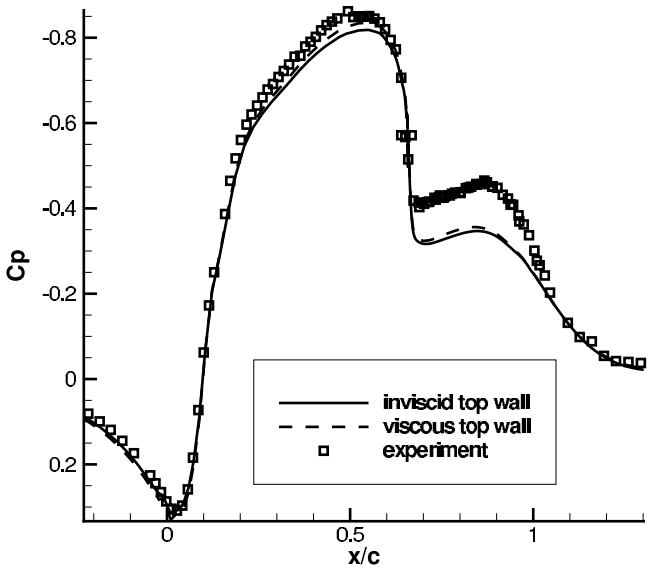

Figure 3: Surface pressure coefficients for no-flow-control case, SA model, medium grid.

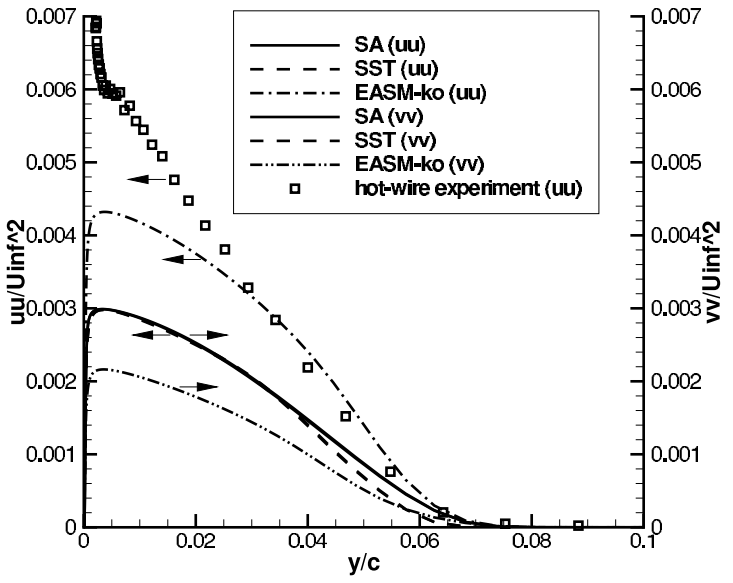

Figure 4: Predicted turbulent normal stresses at $x/c = -2.14$, medium grid.

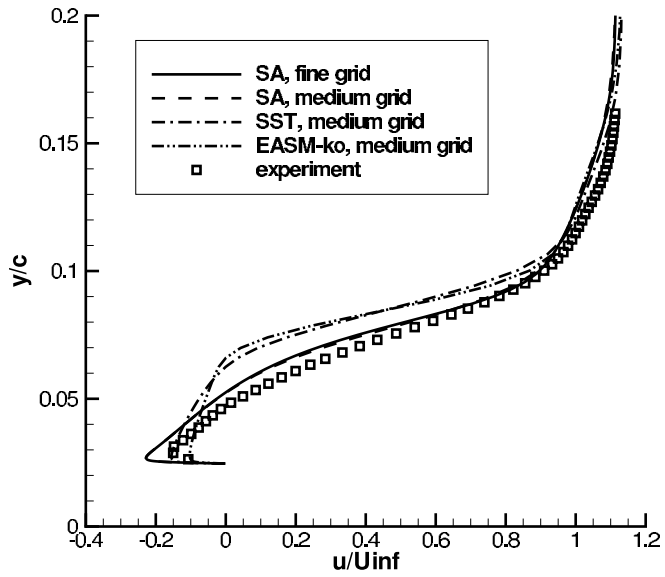

Figure 5: Velocity profiles at $x/c = 0.8$ for the suction case.

[3] Menter, F. R., "Two-Equation Eddy-Viscosity Turbulence Models for Engineering Applications," *AIAA Journal*, Vol. 32, No. 8, 1994, pp. 1598–1605.

[4] Menter, F. R., Rumsey, C. L., "Assessment of Two-Equation Turbulence Models for Transonic Flows," AIAA Paper 94-2343, Colorado Springs, CO, 1994.

[5] Rumsey, C. L., Gatski, T. B., "Summary of EASM Turbulence Models in CFL3D With Validation Test Cases," NASA/TM-2003-212431, June 2003.